Spectrochimica Acta Part A: Molecular and Biomolecular Spectroscopy 138 (2015) 434–440

Contents lists available at ScienceDirect

Spectrochimica Acta Part A: Molecular and Biomolecular Spectroscopy

journal homepage: www.elsevier.com/locate/saa

Synthesis, characterization, optical and antimicrobial studies of polyvinyl alcohol–silver nanocomposites

K.H. Mahmoud *

Physics Department, Faculty of Science, Taif University, Taif, Saudi Arabia
Physics Department, Faculty of Science, Cairo University, Cairo, Egypt

HIGHLIGHTS

- Silver nanoparticles were synthesized by chemical reduction method.
- TEM studies showed that the average particle size of Ag NPs was about 19 nm.
- Optical band gap of PVA was reduced under addition of Ag NPs.
- The antimicrobial activity of PVA was enhanced under addition of Ag NPs.

GRAPHICAL ABSTRACT

TEM image of the Ag colloids.

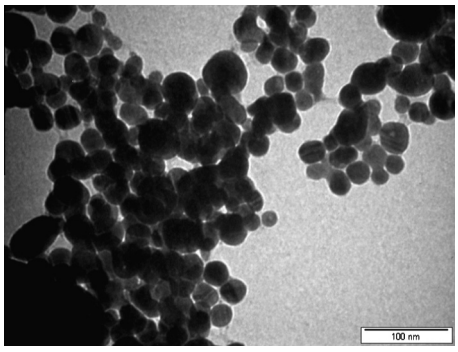

ARTICLE INFO

Article history:
Received 9 August 2014
Received in revised form 23 October 2014
Accepted 24 November 2014
Available online 28 November 2014

Keywords:
Silver nanoparticles
PVA
Optical properties
Antimicrobial activity

ABSTRACT

Silver nanoparticles (Ag NPs) were synthesized by chemical reduction of silver salt ($AgNO_3$) through sodium borohydride. The characteristic surface plasmon resonance band located at around 400 nm in the UV–Visible absorption spectrum confirmed the formation of Ag nanoparticles. Polyvinyl alcohol–silver (PVA–Ag) nanocomposite films were prepared by the casting technique. The morphology and interaction of PVA with Ag NPs were examined by transmission electron microscopy and FTIR spectroscopy. Optical studies show that PVA exhibited indirect allowed optical transition with optical energy gap of 4.8 eV, which reduced to 4.45 eV under addition of Ag NPs. Optical parameters such as refractive index, complex dielectric constant and their dispersions have been analyzed using Wemple and DiDomenco model. Color properties of the nanocomposites are discussed in the framework of CIE L*u*v* color space. The antimicrobial activity of the nanocomposite samples was tested against Gram positive bacteria (*Staphylococcus aureus* NCTC 7447 & *Bacillus subtillis* NCIB 3610), Gram negative bacteria (*Escherichia coli*, NTC10416 & *Pseudomonas aeruginosa* NCIB 9016) and fungi (*Aspergillus niger* Ferm – BAM C-21) using the agar diffusion technique. The antimicrobial study showed that PVA has moderate antibacterial activity against *B. subtillis* and the 0.04 wt% Ag NPs composite sample effect was strong against *S. aureus*.

Introduction

Metal nanoparticles particles posses peerless electronic, optical, magnetic, thermal and catalytic properties that differ extremely

* Address: Physics Department, Faculty of Science, Taif University, Taif, Saudi Arabia. Tel.: +966 530175838.
E-mail address: cairouni1@yahoo.com

http://dx.doi.org/10.1016/j.saa.2014.11.074
1386-1425/

from that of the bulk phase [1–3]. Polymer based nanocomposites are being considered as versatile materials in many scientific applications leading to technological progress [4,5]. This is due to the fact that incorporation of the nanoparticles into the polymer matrix significantly affects its optical, thermal and electrical properties [6,7] while retaining its ingrained characteristics. It opens a new gateway in developing the materials for improved performance [8] in many potential applications like optical devices, biomedical science, the efficient integration of such nanocomposites for technological applications, the pre-requisites include the selection of host matrix and embedded nanoparticles along with the control on their size, shape, concentration and distribution within the matrix [9–11].

Silver nanoparticles (Ag NPs) have received considerable attention due to its chemical stability, good thermal, electrical conductivity and catalytic properties. Different methods can be used for Silver nanoparticles synthesis such as chmical, electrical [9], γ- radiation [12], photochemical [13], laser ablation [14].

Polyvinyl alcohol polymer is a suitable host matrix due to its high mechanical strength, water-solubility, good environmental stability, easy processability, Besides, it is semicrystalline, fully biodegradable, bio compatible, non toxic. Moreover, it contains a carbon backbone with hydroxyl groups, which can be used as a source of hydrogen bonding and assist in the formation of polymer nanocomposites [15–18].

Silver nanoparticles gained a great attention for its antimicrobial and beneficial properties toward health since ancient times [19]. These nanoparticles also are antimicrobial regarding a broad spectrum of Gram-negative and Gram-positive bacteria [20,21]. Moreover, silver nanoparticles show antifungal [22] and antiviral activity [23,24]. Recently, the attractive antibacterial activities of silver nanoparticles have retrieved importance due to an increase of bacterial resistance to antibiotics caused by their excessive use. The antibacterial activity of the silver-containing materials can be used, for example, in medicine to reduce infections as well as to prevent bacterial colonization on prostheses, dental materials, vascular grafts, catheters, human skin, and stainless steel materials [25].

As a result of coagulation of the metal colloids, they are usually unstable and difficult to use and consequently, their antibacterial activities are poor. This problem can be greatly solved by implanting or encapsulating the metal nanoparticles with polymer matrices [26,27]. PVA could be considered as a good host material for metal, due to its above foregoing properties [15–18] which make the silver nanoparticles can be easily prepared in aqueous medium and the preparation is virtually non-toxic.

In this work, we have attempted the preparation of PVA–Ag nanocomposites. We will focus our attention to enhance optical, structural, and antimicrobial properties of nanocomposites.

Experimental

Preparation of samples

Poly(vinyl)alcohol (PVA) with an approximate molecular weight of 17,000 was supplied by BDH chemical Ltd. Poole England. Silver nitrate and sodium borohydride (Fisher) were used as received. All glassware were thoroughly cleaned in aqua- regia and rinsed copiously with triply distilled water. All solutions of the salts and polymer were prepared in triply distilled water. Hydrosol of silver nanoparticles has been chemically synthesized by chemical reduction of silver nitrate through sodium borohydride [28]. For this 10 mL volume of 1.0 mM $AgNO_3$ was added drop wise to 30 mL of 2.0 mM sodium borohydride solution that had been cooled in an ice bath. The reaction mixture was stirred vigorously on a magnetic stir plate. The solution turned light yellow after the addition of 2 mL of silver nitrate and a brighter yellow when all of the silver nitrate had been added. The entire addition took about three minutes, after which the stirring was stopped and the stir bar removed. The clear yellow colloidal silver is stable at room temperature stored in a transparent vial for as long as several weeks or months. Upon aggregation the colloidal silver solution turns darker yellow, violet and then grayish.

Weighed amounts of PVA were dissolved in triply distilled water using a magnetic stirrer at 60 °C. Solutions of silver colloids and PVA were mixed using a magnetic stirrer at 60 °C with different weight percentages (0, 0.04, 0.06 and 0.08 wt% silver colloids). The solid samples were made by casting technique. Films of suitable thickness (≈100 μm) were cast onto stainless steel Petri dishes, and then dried in an open air at room temperature (30 °C) for 3 days until solvent was nearly evaporated.

Spectroscopic measurements

Transmission electron microscopy (TEM) was performed using Joel "JEM-1011" electron microscope operated at 80 kV. The IR spectra were measured using PYE spectrophotometer in the range of 400–4000 cm^{-1}. The absorption measurements of the samples were performed using V-670 spectrophotometer. The tristimulus transmittance values (X, Y, Z) were calculated using the transmittance data obtained in the visible range according to CIEL*u*v* system. Also, the CIE three dimensional (L^*, U^*, V^*) color constants, whiteness (W), yellowness (Y), chroma (C^*), hue and color difference (ΔE) were studied.

Antimicrobial activity

The antimicrobial activity of the nanocomposite samples was determined using the agar disc diffusion method as described by the National Committee for Clinical Laboratory Standards (NCCLS) [29–31]. The antibacterial activities were done by using 1 mg/ml solution in dimethyl formamide (DMF). The tested organisms were, Gram positive bacteria (*Staphylococcus aureus* NCTC 7447 & *Bacillus subtillis* NCIB 3610), Gram negative bacteria (*Escherichia coli*, NTC10416 & *Pseudomonas aeruginosa* NCIB 9016) and fungi (*Aspergillus niger* Ferm – BAM C-21). The bacteria and fungi were maintained on nutrient agar medium and Czapek Dox agar medium respectively. DMF showed no inhibition zones. The agar media were inoculated with different test microorganisms. After 24 h, of incubation at 30 °C for bacteria and 48 h of incubation at 28 °C for fungi, the diameter of inhibition zone (mm) was measured. We will Briefly, describe the agar well diffusion. With a sterile loop, pure colonies of the bacterial cultures were picked up; the colonies were suspended in 5 ml of sterile physiological saline. Well containing the biomaterial were placed a sterile forceps onto the agar surface and gently pressed down to ensure contact the plates were pre-incubated for 1 h, at refrigerator followed by incubation at 37 °C for 24 h, after incubation, the diameter of inhibition zone were measured (including the diameter of the hole).

Results and discussion

TEM profiles and IR spectra

Fig. 1(a) shows TEM image of silver nanoparticles colloidal solution with spherical three dimensional distributions and average particle size 19 nm. For 0.08 wt% Ag NPs- PVA composite sample (Fig. 1(b)) the nanoparticles are more dispersed in PVA and the particle size increased up to ≈33 nm. The polymer functions as a binder and also it prevents the process of agglomeration

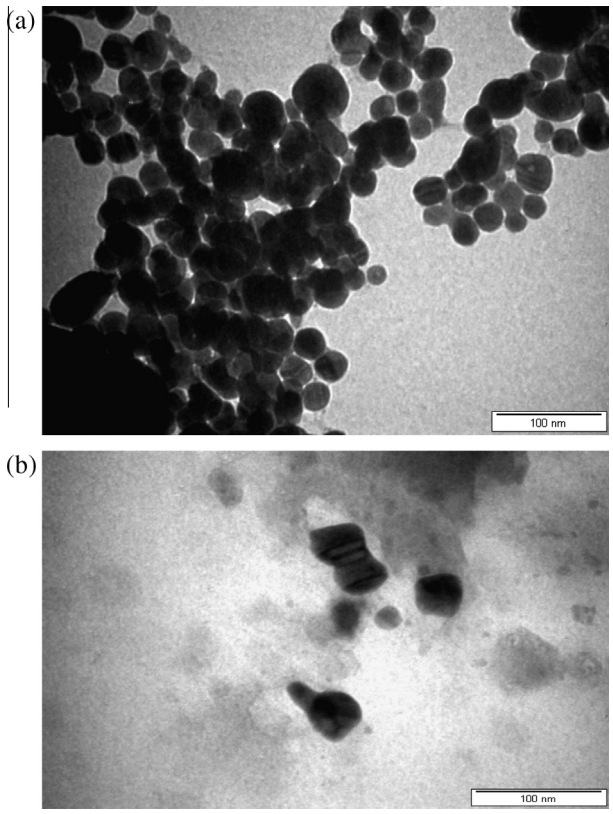

Fig. 1. TEM image of the (a) Ag colloids, (b) 0.08 wt% Ag NPs doped PVA sample.

of Ag NPs [32] and finally limits the diameter of nanoparticles formed. The electrostatic interactions between PVA and silver nanoparticles were studied by FTIR spectroscopy (Fig. 2). In case of PVA there is a strong broadband at 3360–3280 cm^{-1} which is assigned to O—H stretching frequency indicating the presence of hydroxyl groups. The bands observed at 2920 and 1740 cm^{-1} correspond to C—H and C=O stretching vibrations, respectively and the absorption band at 1670 cm^{-1} arises due to C=C stretching [33]. The absorption bands at 1430 cm^{-1} is assigned to CH_2 bending and that at 1380 cm^{-1} is due to CH_2 wagging [34]. The bands appeared at 1250 cm^{-1} and 1003 cm^{-1} is due to C—H wagging and C—O stretching respectively. The absorption band appeared at 852 cm^{-1} is due to the out-of-plane vibration of C—H group [22]. An important band centered at 947 cm^{-1} symbolizes the presence of the syndiotactic structure of PVA [35] suggesting the regular inter-chain bridging in a layered structure via sequential distribution of OH groups, conferring the H-bonding functionality to planarize the polymer backbone [36]. However, decrease in the intensity of this band with increasing concentration of Ag nanoparticles ascertain the loss of such planer structure leading to an abundance of delocalized n-electrons causing enhanced optical, thermal, and electrical properties [36,37]. Comparing the spectra of nanocomposite samples to that of pure PVA, it is observed that with increase in Ag NPs concentration, a clear reduction in the intensity of the band involved in H-bonding between PVA chains (3360–3280 cm^{-1}) and blue shifting of the band at 2920 cm^{-1} (CH_2 asymmetric stretch), corroborating the formation of hydrogen bonds between the PVA chains and embedded Ag NPs. Also the complete disappearance of the band at 1670 cm^{-1} and decrease in intensity of the band at 1740 and 852 cm^{-1} suggest the formation of chemical conjugation of Ag nanoparticles with PVA molecules. Finally the continuous decrease in intensities of bands in region 1440–1250 cm^{-1} indicates the decoupling between OH and CH vibrations due to electrostatic interaction between OH and embedded silver nanoparticles. All the foregoing observed changes clearly suggest the possibility of complexation between Ag nanoparticles and PVA.

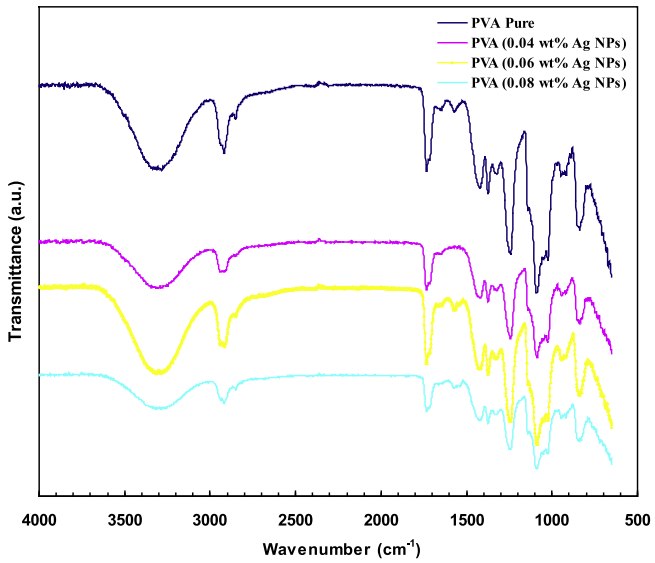

Fig. 2. FTIR spectra of PVA–silver nanocomposites.

Optical study

Optical absorbance spectra

The UV–visible extinction spectrum of the colloidal dispersion of Ag NPs (Fig. 3(a)) shows an intense broad absorption peak

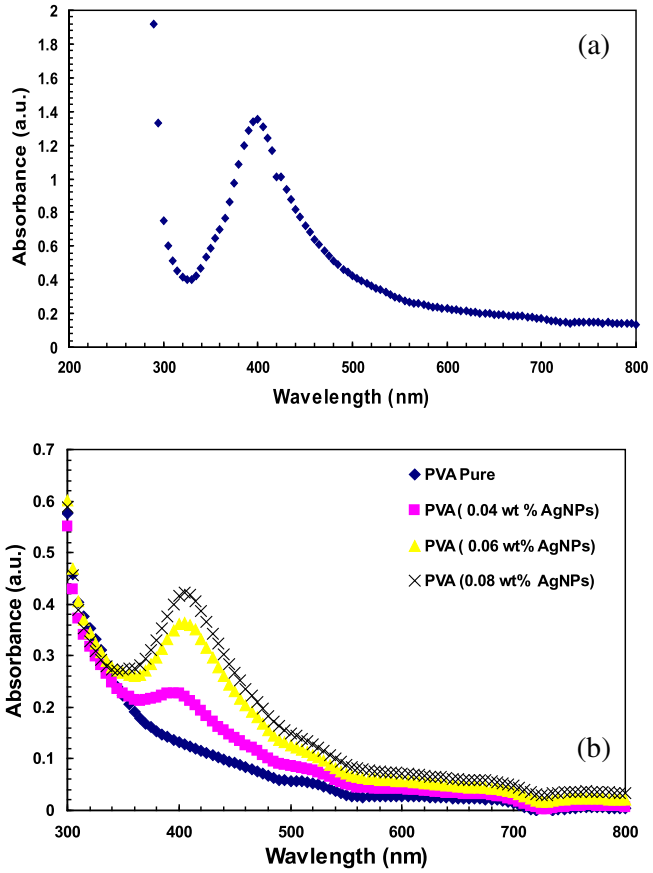

Fig. 3. UV–Visible spectra of (a) Ag colloids, (b) PVA–silver nanocomposites.

around 400 nm due to surface plasmon resonance (SPR) of silver nanoparticles [38]. The electric field of the incident electromagnetic radiation displaces the electrons of particles from equilibrium and, in turn, produces a restoring force that results in oscillatory motion of the electrons with a characteristic frequency namely, SPR frequency. At the same time, the oscillatory electrons induce polarization of the opposite direction in the surrounding medium, and this polarization reduces the restoring force for the electrons thereby shifting the SPR to a lower frequency. The SPR wavelengths (Fig. 3(b)), are found to be at 400, 404 and 405 nm for 0.04, 0.06 and 0.08 wt% Ag NPs doped PVA samples respectively. The red shift of SPR wavelength can be attributed to the increased dielectric constant of PVA and this is an indication of increased particle size [39]. The SPR wavelength can be modulated via the material, size, geometry, and filling factor of the nanoparticle arrays, as well as the dielectric constant of environment. The SPR modulation can be used in chemical assays in which varying the concentration of an analyte causes a predictable wavelength shift [40].

Optical parameters

The absorption coefficient, α (ν) below and near the edge of each curve was determined, using the relation [41]

$$\alpha(\nu) = \frac{-1}{d} \ln \left[\frac{-(1-R)^2}{2TR^2} + \sqrt{\frac{(1-R)^4}{4T^2R^4} + \frac{1}{R^2}} \right]. \quad (1)$$

where d is the thickness of the film sample; R is the reflectance; T is the transmittance of the sample for incident photon at frequency ν.

The observed shift in the fundamental absorption edge of UV–Visible spectra can be correlated with the optical band gap by Tauc's expression [42]

$$\alpha(\nu)h\nu = C(h\nu - E_{opt})^n \quad (2)$$

where C is constant called a band tailing parameter; E_{opt} is the optical band gap energy; n is the index, which takes different values depending on the mechanism of interband transitions $n = 2, 3, 1/2, 1/3$ corresponding to indirect allowed, indirect forbidden, direct allowed and direct forbidden transitions, respectively.

The values of the optical band gap E_{opt} can be deduced from the intercept of the linear fitted lines in the plots of $(\alpha h\nu)^{1/2}$ versus $h\nu$, as shown in Fig. 4. The values of the optical band gap so determined are listed in Table 1. It is observed that there is a reduction in the optical band gap of pure PVA(4.80 eV) under addition of silver nanoparticles and reached to 4.45 eV in 0.08 wt% Ag NPs doped PVA sample. Such decrease in the value of E_{opt} can be attributed to the formation of bonds between silver nanoparticles and PVA molecules. Therefore, the trap levels between the HOMO and LUMO energy states are formed and make the lower energy transitions feasible and results in the reduction of optical band gap [43]. Further, the values of the optical band gap, E_{opt}, can be correlated to the number of carbon atoms per molecule through the expression [44]

$$E_{opt} = 34.3\sqrt{M} \quad (3)$$

where M is the number of carbon atoms in a carbonaceous cluster. The calculated values of M for PVA and its nanocomposites are tabulated in Table 1. The value of M for PVA, which is around 51, increases to 59 in 0.08 wt% Ag NPs composite sample. Such an increase can be correlated to the increased conjugation the in monomer units [44] of PVA matrix after the embedding of silver nanoparticles, which leads to an increase in the number of carbon atoms taking part in carbonaceous cluster in PVA–Ag nanocomposites.

Table 1
Values of optical band gap (E_{opt}), number of carbon atoms (M) per carbonaceous cluster and refractive index (n_o) for PVA–silver nanocomposites.

wt% Ag NPs	E_{opt} (eV)	M	n_o
0.00	4.80	~51	1.52
0.04	4.62	~55	1.77
0.06	4.60	~56	1.88
0.08	4.45	~59	1.91

Dispersion of refractive index

The refractive index is one of the fundamental properties in material, because it is closely related to the electronic polarizability of ions and the localized field inside the material [45]. Estimation of the refractive indices of optical materials is important for applications in integrated optics devices such as switches, filters, and modulators. The values of refractive index n and extinction coefficient k have been calculated using the theory of reflectivity of light [46]

$$R = \frac{[(n-1)^2 + k^2]}{[(n+1)^2 + k^2]} \quad (4)$$

where $k = \alpha\lambda/4\pi$ is the extinction coefficient of the material; λ is the wavelength of the incident photon. The values of n at different wavelengths are plotted in Fig. 5. It is evident that the refractive index decreases with increasing wavelength of incident photon

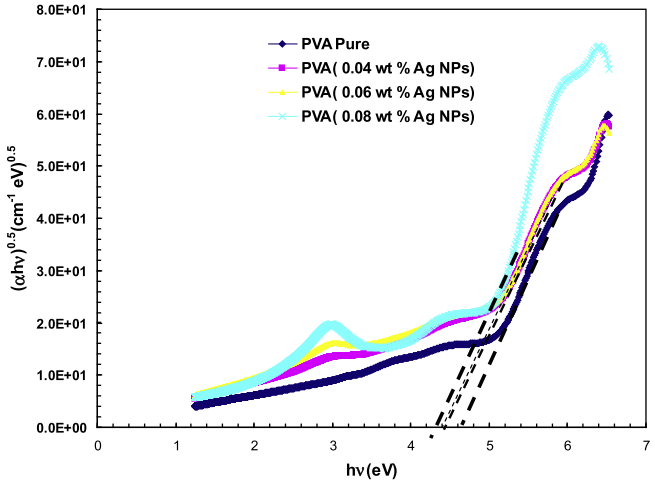

Fig. 4. Tauc's Plot of PVA–silver nanocomposites.

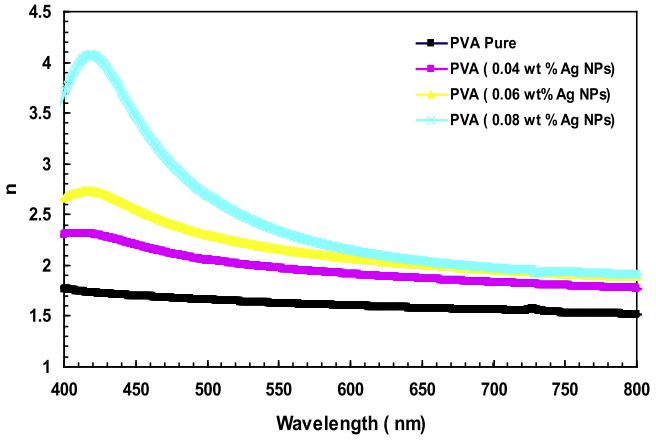

Fig. 5. Variation of refractive index n with wavelength for PVA–silver nanocomposites.

and finally, almost saturates at values n_0 (longer wavelength values) (see Table 1) for PVA as well as for its nanocomposites.

It is also clear that as the concentration of silver nanoparticles increases, the refractive index increases and this can be explained in terms of Bhar and Pinto model [47]. According to this model, the increase in the refractive index of nanocomposite samples is explained in terms of increased density of nanocomposites with increasing concentration of fillers. The increased density of the PVA after addition of Ag NPs may be due to the formation of intermolecular bonding between the embedded silver nanoparticles and the adjacent OH groups of PVA through electrostatic interaction and this is confirmed earlier through the FTIR spectroscopy.

Neglecting the lattice contribution, for a wavelength longer than the phonon resonance, Wemple and DiDomenco [48,49] have examined the refractive index data below the inter-band absorption edge. They found that the normal dispersion of the optical dielectric constant in materials and the energy dependence of refractive index satisfy a Sellmeier relation of the form

$$n^2(E) = 1 + \frac{E_{osc}E_d}{E_{osc}^2 - E^2} \tag{5}$$

where E_{osc} is the single oscillator energy (average oscillator energy for electrons); E is the photon energy in eV; E_d is the dispersion energy parameter of the material. The parameter E_{osc} is directly related to the optical band gap. The parameter E_d is a measure of the inter-band optical transitions. Experimental verification of Eq. (5) can be obtained by plotting $(n^2-1)^{-1}$ versus $(h\nu)^2$ as illustrated in Fig. 6(a) which yields a straight line for normal behavior and allows the determination of oscillator parameters (Table 2).

The refractive index at infinite wavelength (n_∞), average oscillator wavelength (λ_o) and oscillator strength S_o can be calculated through the relation [50]

$$\frac{n_\infty^2 - 1}{n^2 - 1} = 1 - \frac{\lambda_o^2}{\lambda^2} \tag{6}$$

Rearranging Eq. (6) gives

$$n^2 - 1 = \frac{S_o^2 \lambda_o^2}{(1 - \lambda_o^2)/\lambda^2} \tag{7}$$

where $S_o = (n_\infty^2 - 1)/\lambda_0^2$. The values of n_∞ and S_o are derived from a linear plot of $(n^2-1)^{-1}$ versus $1/\lambda^2$ as shown in Fig. 6(b) and the data are presented in Table 2. It is observed that these parameters change noticeably with composition. The obtained curves in Fig. 6(a and b) show positive deviation from linearity. A positive deviation from linearity at longer wavelengths is usually observed due to the negative contribution of lattice vibrations on the refractive index.

Table 2
Single oscillator model parameters for PVA–silver nanocomposites.

wt% Ag NPs	E_d (eV)	E_{osc} (eV)	n_∞	ε'_∞	λ_o (nm)	S_o (nm^{-2})
0.00	11.70	6.18	1.70	2.89	200.0	4.69×10^{-5}
0.04	15.30	5.75	1.91	3.64	215.0	5.78×10^{-5}
0.06	20.50	5.99	2.10	4.41	206.0	8.05×10^{-5}
0.08	14.44	5.16	2.20	4.84	239.8	6.67×10^{-5}

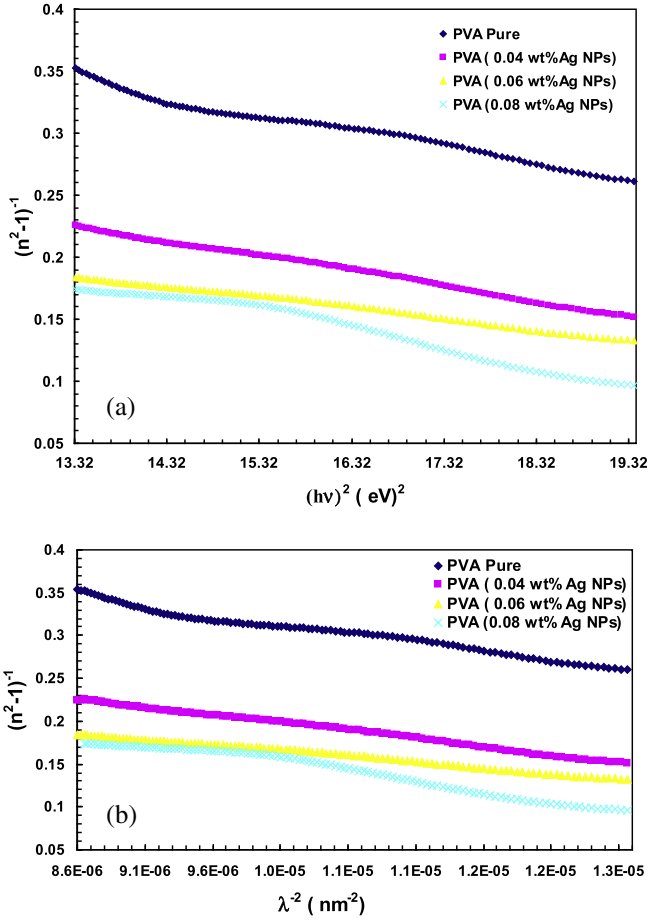

Fig. 6. Plots of the refractive index factor $(n^2-1)^{-1}$ versus (a) $(h\nu)^2$, (b) $(\lambda)^{-2}$ for PVA–silver nanocomposites.

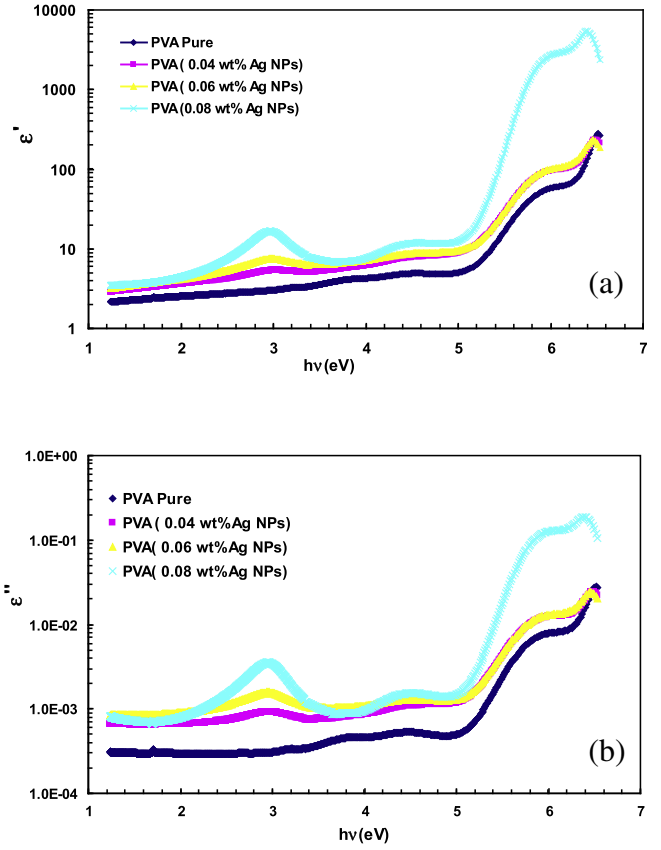

Fig. 7. Plots of (a) dielectric constant (ε'), (b) dielectric loss (ε'') versus photon energy $h\nu$ for PVA–silver nanocomposites.

Complex dielectric constant analysis

The complex dielectric constant can be derived from the following relations [51]

$$\varepsilon'(\lambda) = n^2(\lambda) - k^2(\lambda) \quad (8)$$

$$\varepsilon''(\lambda) = 2n(\lambda)k(\lambda) \quad (9)$$

where ε' and ε'' are real and imaginary parts of dielectric constant respectively and can be calculated for PVA–Ag nanocomposite system at different incident photon energies. From Fig. 7(a and b), it is clear that as incident photon energy increases ε' and ε'' increase and peaked at certain energies. The 0.08 wt% Ag NPs composite sample has the largest ε' and ε'' over the whole energy range. The dielectric constant at infinite wavelengths (ε'_∞) equals the value of n^2_∞ (see Eq. (7)). It is clear that ε'_∞ increases as content of Ag NPs increases (as seen in Table 2). This increase in dielectric constant can be attributed to increase of number of ionizable charges and consequently polarization.

Color properties

Fig. 8 illustrates the variation of the tristimulus transmittance (Y_t) with wavelength in the range of 380–760 nm for nanocomposite samples. It is observed that the behavior of Y_t for all samples is similar and showed the same peak position at about 560 nm. Also it is seen that Y_t (max) increases as Ag NPs content decreases and this was attributed to the transmission values.

Table 3 represents the color parameters L^*, U^*, V^*, h_{ue}, W, Y_e [52] and color difference data, ΔL^*, ΔU^*, ΔV^*, ΔC^*, and ΔE between all samples and pure PVA. It is observed that the color parameters change noticeably with a variation of Ag NPs content in the investigated samples. Moreover, the color difference data indicate that silver nanoparticles have pronounced effect on color parameters. The 0.08 wt% Ag NPs–PVA composite sample is less light, redder, more yellow and more saturated than the other samples. In addition, it has the highest ΔE and h_{ue} values among all the employed nanocomposite samples. The observed changes in the color parameters for PVA–Ag nanocomposite samples may be due to the formation of new dopant centers of PVA.

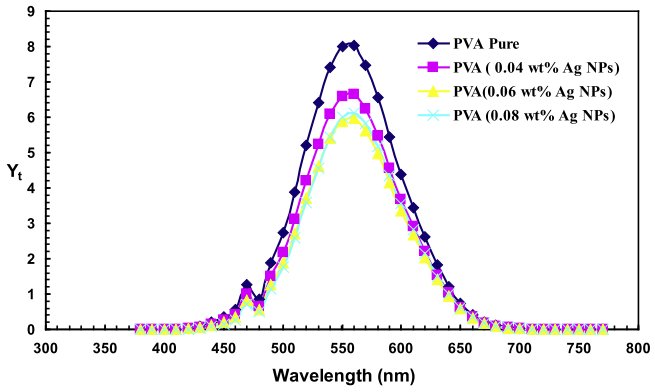

Fig. 8. Tristimulus transmittance of PVA–silver nanocomposites.

Antimicrobial activity

PVA–Ag nanocomposites were tested for antibacterial activity using Gram positive bacteria (*S. aureus* NCTC 7447 & *B. subtillis* NCIB 3610), Gram negative bacteria (*E. coli*, NTC10416 & *P. aeruginosa* NCIB 9016) and fungi (*A. niger* Ferm – BAM C-21). Table 4 shows the inhibition zones that were formed by nanocomposite samples. It is observed that pure PVA exhibited antibacterial activity only against *B. subtillis* and showed no activity towards other microorganisms. The activity of PVA may arise from the hydroxyl groups which may play an important role in the antibacterial activity [53].

The 0.04 wt% Ag NPs composite sample showed better antibacterial activity against *S. aureus* and *E. coli*. It is observed that the nanocomposite samples showed no activity against other microorganisms. The antibacterial activity of silver is dependent on Ag^+ that binds strongly to electron donor groups on biological molecules like sulfur, oxygen or nitrogen. The silver ions act by displacing other essential metal ions such as Ca^{2+} or Zn^{2+} [54]. The concentration of nanoparticles plays an important role in the antibacterial activity, such that, the interaction of particles with the cell wall of bacteria is small at low concentrations. On the other hand, at high concentrations of the particles, the aggregation probability of particles increases, as a result, the effective surface to volume ratio of particles and so the resulting interaction between particles and the cell wall of bacteria decrease. There are various mechanisms on the action of silver nanoparticles on the bacterial cell [55]. Some of these mechanisms were summarized as follows: (i) the ability of silver nanoparticles to anchor to the bacterial cell wall and then penetrate it [56], (ii) the formation of free radicals by the silver nanoparticles, which can damage the cell membrane and make it porous [20], (iii) releasing the silver ions by the nanoparticles, which can interact with the thiol groups of many vital enzymes and inactivate them [57], and (iv) the nanoparticles can modulate the signal transduction in bacteria which stops the growth of bacteria [58].

Table 3
Color parameters for PVA–silver nanocomposites.

wt% Ag NPs	L^*	U^*	V^*	C^*	ΔL^*	ΔU^*	ΔV^*	ΔC^*	ΔE	h_{ue}	W	Y_e
0.00	92.28	1.61	3.54	3.90	–	–	–	–	–	65.47	−973.06	0.04
0.04	85.56	4.06	11.42	12.12	−6.72	2.45	7.88	8.25	10.64	70.41	−803.07	0.14
0.06	81.83	6.55	18.25	19.39	−10.45	4.94	14.71	15.51	14.07	70.25	−718.07	0.23
0.08	80.19	12.03	36.76	38.68	−12.09	10.42	33.22	34.81	36.24	71.88	−726.29	0.45

Table 4
Antimicrobial activity for PVA–silver nanocomposites.

wt% Ag NPs	*Bacillus subtillis*	*Staphylococcus aureus*	*Escherichia coli*	*Pseudomonas aeruginosa*	*Aspergillus niger*
0.00	11	–	–	–	–
0.04	–	17	18	–	–
0.06	–	–	–	–	–
0.08	–	–	–	–	–

Gram-positive bacteria possess a thick cell wall containing many layers of peptidoglycan and teichoic acids, but in contrast, Gram negative bacteria have a relatively thin cell wall consisting of a few layers of peptidoglycan surrounded by a second lipid membrane containing lipopolysaccharides and lipoproteins.

These differences in cell wall structure play an important role in antibacterial susceptibility, so some antibiotics can kill only Gram-positive bacteria and is ineffective against Gram-negative pathogens [59].

Conclusions

Silver nanoparticles had been synthesized by the chemical reduction method of silver salt ($AgNO_3$) through sodium borohydrid. UV–vis and TEM techniques confirmed the synthesized nanoparticles. Silver nanoparticles can successfully dope and enhance color and optical properties of PVA. The prepared nanocomposite samples showed good antibacterial activity against *B. subtillis*, *S. aureus* and *E. coli*. The above results may enable us to adjust and use these material properties for selected practical applications.

References

[1] L.N. Lewis, Chem. Rev. 93 (1993) 2693.
[2] A.P. Alivisatos, Science 271 (1996) 933.
[3] L.M. Liz-Marzán, Mater. Today 7 (2004) 26.
[4] W. Wu, S. Liang, L. Shen, Z. Ding, H. Zheng, W. Su, L. Wu, J. Alloys Compd. 520 (2012) 213.
[5] E. Badamshina, M. Gafurova, J. Mater. Chem. 22 (2012) 9427.
[6] S. Mahendia, A.K. Tomar, S. Kumar, Mater. Sci. Eng., B 176 (2011) 530.
[7] S. Mahendia, A.K. Tomar, S. Kumar, J. Alloys Compd. 508 (2010) 406.
[8] S. Sultana, Rafiuddin, M.Z. Khan, K. Umar, J. Alloys Compd. 535 (2012) 44.
[9] P.P. Jeeju, A.M. Sajimol, V.G. Sreevalsa, S.J. Varma, S. Jayalekshmi, Polym. Int. 60 (2011) 1263.
[10] S.H. Jeon, P. Xu, B. Zhang, N.H. Mack, H. Tsai, L.Y. Chiang, H.L. Wang, J. Mater. Chem. 21 (2011) 2550.
[11] R.D. Peng, H.W. Zhou, H.W. Wang, L. Mishnaevsky Jr., Comput. Mater. Sci. 60 (2012) 19.
[12] S.H. Choi, Y.P. Zhang, A. Gopalan, K.P. Lee, H.D. Kang, Colloid. Surface A 256 (2005) 165.
[13] Z. Li, Y. Li, X.F. Qian, J. Yin, Z.K. Zhu, Appl. Surf. Sci. 250 (2005) 109.
[14] T. Tsuji, N. Watanabe, M. Tsuji, Appl. Surf. Sci. 211 (2003) 189.
[15] R.F. Bhajanti, V. Ravindrachary, A. Harisha, G. Ranganathaiah, G.N. Kumaraswamy, Appl. Phys. A 87 (2007) 797.
[16] M.H. Harun, E. Saion, A. Kassim, E. Mahmud, M.Y. Hussain, I.S. Mustafa, J. Adv. Sci. Arts 1 (2009) 9.
[17] E. Tuncer, I. Sauers, D.R. James, A.R. Ellis, M.P. Paranthaman, A. Goyal, K.L. More, Nanotechnology 18 (2007) 325704.
[18] K.H. Mahmoud, Z.M. El-Bahy, A.I. Hanafy, J. Phys. Chem. Solids 72 (2011) 1057.
[19] S. Silver, T.L. Phung, G. Silver, J. Ind. Microbial. Biotechnol. 33 (2006) 627.
[20] J.S. Kim, E. Kuk, K.N. Yu, J.H. Kim, S.J. Park, H.J. Lee, S.H. Kim, Y.K. Park, Y.H. Park, C.Y. Hwang, Y.K. Kim, Y.S. Lee, D.H. Jeong, M.H. Cho, Nanomedicine 3 (2007) 5.
[21] A. Pancek, L. Kvitek, R. Prucek, M. Kolar, R. Vecerova, N. Pizúrova, V.K. Sharma, T. Nevecna, R. Zboril, J. Phys. Chem. B 110 (2006) 16248.
[22] K.J. Kim, W.S. Sung, S.K. Moon, J.S. Choi, J.G. Kim, D.G. Lee, J. Microbiol. Biotechnol. 18 (2008) 1482.
[23] J.L. Elechiguerra, J.L. Burt, J.R. Morones, A. Camacho-Bragado, X. Gao, H.H. Lara, M.J. Yacaman, J. Nanobiotechnol. 3 (2005) 1.
[24] L. Lu, R.W.Y. Sun, R. Chen, C.K. Hui, C.M. Ho, J.M. Luk, G.K.K. Lau, C.M. Che, Antivir. Ther. 13 (2008) 253.
[25] A. Panacek, L. Kvitek, R. Prucek, J. Phys. Chem. B. 110 (2006) 16248.
[26] Z.H. Mbhele, M.G. Salemane, C.G.C.E. van Sittert, Chem. Mater. 15 (2003) 5019.
[27] K.S. Chou, C.Y. Ren, Mater. Chem. Phys. 64 (2000) 241.
[28] Y. Fang, J. Chem. Phys. 108 (1998) 4315.
[29] K.E. Cooper, F.W. Kavanagh, An analytical Microbiology, vol. I, II, Academic Press, New York and London, 1972.
[30] National Committee for Clinical Laboratory Standards, NCCLS document M7-A4, fourth ed., Wayne, Pa: National Committee for Clinical Laboratory Standards, Methods for dilution antimicrobial susceptibility tests for bacteria that grow aerobically, Approved standard, 1997.
[31] National Committee for Clinical Laboratory Standards, Performance standards for antimicrobial disk susceptibility tests, sixth ed., approved standard M2-A6, Wayne, Pa: National Committee for Clinical Laboratory Standards, 1997.
[32] K.A. Bogle, S.D. Dhole, V.N. Bhoraskar, Nanotechnolgy 17 (2006) 3204.
[33] C.A. Finch, Polyvinyl Alcohol Properties and Application, John Wiley and Sons, 1973.
[34] S. Mahendia, A.K. Tomar, P.K. Goyal, S. Kumar, J. Appl. Phys. 113 (2013) 073103.
[35] V. Giménez, A. Mantecón, V. Cádiz, J. Polym. Sci. Part A: Polym. Chem. 34 (1996) 925.
[36] P.B. Bhargav, V.M. Mohan, A.K. Sharma, V.V.R.N. Rao, Int. J. Polym. Mater. 56 (2007) 579.
[37] M. Abdelaziz, M.M. Ghannam, Phys. B 405 (2010) 958.
[38] L.M. Liz-Marzán, Langmuir 22 (2006) 32.
[39] A.J. Haes, W.P. Hall, L. Chang, W.L. Klein, R.P. Van Duyne, Nano Lett. 4 (2004) 1029.
[40] David D. Evanoff Jr., G. Chumanov, Chem. Phys. Chem. 6 (2005) 1221.
[41] R. Valalova, L. Tichy, M. Vlcek, H. Ticha, Phys. Status Solid. A 181 (2000) 199.
[42] E.A. Davis, N.F. Mott, Phil. Mag. 22 (1970) 903.
[43] R.P. Chahal, S. Mahendia, A.K. Tomar, S. Kumar, Dig. J. Nanomater. Bios. 6 (2011) 299.
[44] D. Fink, W.H. Chung, R. Klett, A. Schmoldt, J. Cardoso, R. Montiel, M.H. Vazquez, L. Wang, F. Hosoi, H. Omichi, P.G. Langer, Radiat. Eff. Def. Solids 133 (1995) 193.
[45] N. Singth, P.K. Khanna, Mater. Chem. Phys. 104 (2007) 367.
[46] D.P. Gosain, T. Shimizu, M. Ohmura, M. Suzuki, T. Bando, S. Okano, J. Mater. Sci. 26 (1991) 3271.
[47] O. Bhar, J.C. Pinto, J. Appl. Polym. Sci. 42 (1991) 2795.
[48] M. DiDomenico, S.M. Wemple, J. Appl. Phys. 40 (1946) 720.
[49] S.H. Wemple, M. DiDomenico, Phys. Rev. B 3 (1971) 1338.
[50] F. Yakuphanoglu, M. Durmus, M. Okutan, O. Koysal, V. Ahsen, Phys. B 373 (2006) 262.
[51] A.A. Al-Ghamdi, Vacuum 80 (2006) 400.
[52] D.L. Macadam, Color Measurements: Theme and Variation, Springer Series in Optical Sciences Springer – Verlag, Berlin Heidelberg New York, 1981.
[53] N. Sari, S. Arslan, E. Logoglu, I. Sakiyan, G.U. J. Sci. 16 (2003) 283.
[54] P. Boomi, H.G. Prabu, J. Mathiyarasu, Colloids Surf. B 103 (2013) 9.
[55] S. Prabhu, E.K. Poulose, Int. Nano Lett. 2 (2012) 1.
[56] I. Sondi, B. Salopek-Sondi, J. Colloid Interface Sci. 275 (2004) 177.
[57] Q.L. Feng, J. Wu, G.Q. Chen, F.Z. Cui, T.N. Kim, J.O. Kim, J. Biomed. Mater. Res. 52 (2008) 662.
[58] S. Shrivastava, T. Bera, A. Roy, G. Singh, P. Ramachandrarao, D. Dash, Nanotechnology 18 (2007) 225103.
[59] A.L. Koch, Clin. Microbiol. Rev. 16 (2003) 673.